Article

Thermal Atomic Layer Deposition of Yttrium Oxide Films and Their Properties in Anticorrosion and Water Repellent Coating Applications

Christian Dussarrat [1,*], Nicolas Blasco [2], Wontae Noh [3], Jooho Lee [3], Jamie Greer [1], Takashi Teramoto [1], Sunao Kamimura [1], Nicolas Gosset [1] and Takashi Ono [1]

[1] Air Liquide Laboratories, Tokyo Innovation Campus, 2-2 Hikarinooka, Yokosuka, Kanagawa 239-0847, Japan; Jamie.greer@airliquide.com (J.G.); takashi.teramoto@airliquide.com (T.T.); sunao.kamimura@airliquide.com (S.K.); nicolas.gosset@airliquide.com (N.G.); takashi.ono@airliquide.com (T.O.)

[2] Air Liquide Advanced Materials, 3121 Route 22 East, Branch Estates, Suite 200, Branchburg, NJ 08876, USA; nicolas.blasco@airliquide.com

[3] Air Liquide Laboratories Korea, 50 Yonsei-ro, Sinchon-dong, Seodaemun-gu, Seoul 03722, Korea; wontae.noh@airliquide.com (W.N.); jooho.lee@airliquide.com (J.L.)

* Correspondence: christian.dussarrat@airliquide.com

Abstract: The thermal atomic layer deposition (ThALD) of yttrium oxide (Y_2O_3) was developed using the newly designed, liquid precursor, $Y(EtCp)_2(^iPr_2\text{-amd})$, as the yttrium source in combination with different oxygen sources, such as ozone, water and even molecular oxygen. Saturation was observed for the growth of the Y_2O_3 films within an ALD window of 300 to 450 °C and a growth per cycle (GPC) up to 1.1 Å. The resulting Y_2O_3 films possess a smooth and crystalline structure, while avoiding any carbon and nitrogen contamination, as observed by X-ray photoelectron spectroscopy (XPS). The films showed strong resistance to fluorine-containing plasma, outperforming other resistant materials, such as silicon oxide, silicon nitride and alumina. Interestingly, the hydrophilic character exhibited by the film could be switched to hydrophobic after exposure to air, with water contact angles exceeding 90°. After annealing under N_2 flow at 600 °C for 4 min, the hydrophobicity was lost, but proved recoverable after prolonged air exposure or intentional hydrocarbon exposure. The origin of these changes in hydrophobicity was examined.

Keywords: heteroleptic precursor; thermal atomic layer deposition; yttrium oxide; plasma-resistant coating; water contact angle

1. Introduction

Yttria offers properties that are attractive for a variety of industrial applications. Bulk Y_2O_3 has a high thermal conductivity (0.27 W cm^{-1} K^{-1} at 300 K) and a high melting point (2430 °C). Its refractive index of about 1.9 also allows it to be used in the fabrication of planar waveguides for high-power lasers [1,2]. Yttria already has a wide range of applications in electronics and related fields [3,4]. For example, thin films of yttrium-based oxides, in combination with zirconium oxide, are useful as high-k gate dielectrics due to the large intrinsic band gap in the range of 5.5 to 5.8 eV, which displays improved electrical properties on current commercial examples (e.g., lower leakage current) [5]. Moreover, Y_2O_3 thin films have been employed as optical, anticorrosive coatings and dielectric insulators in electroluminescent devices, such as light-emitting diodes (LEDs), in which metals such as Eu, Er, Tb and Yb have already been applied as dopants [6]. In the field of emerging energy devices, yttrium-stabilized zirconia (YSZ) and yttrium-doped ceria (YDC) are useful as solid-state electrolytes for solid oxide fuel cells (SOFCs) [7,8]. Particularly interesting properties of yttria are its good wear resistance, high mechanical and dielectric strength, as well as strong corrosion and chemical resistance, making it ideal for wear-resistant

coatings in plasma equipment [9]. For such applications, silicon oxide and aluminum oxide are commonly used to shield ceramic components in etchers and plasma-enhanced chemical vapor deposition (PECVD), equipment used in semiconductor processing [10,11]. As semiconductor manufacturing continues to scale down, these materials are becoming increasingly exposed to higher density plasma, which causes faster erosion and ultimately leads to the formation of contaminating particles and defects, resulting in yield loss. Y_2O_3 is now being considered for this application, as its resistance to erosion and degradation is much higher than conventional coatings [12–17]. In addition, Y_2O_3 has already been applied as a hydrophobic layer in various industrial components. Metal oxide hydrophobic coatings are of increasing interest as they exhibit better mechanical durability and thermal stability than organic hydrophobic coatings, properties essential for their use in electronics-related applications, such as in microelectromechanical systems (MEMS) manufacturing.

Y_2O_3 deposition can be achieved by various methods, such as physical vapor deposition (PVD), thermal or plasma-enhanced chemical vapor deposition (CVD) and related variations on atomic layer deposition (ALD). In recent decades, Y_2O_3 studies have shown that important film properties, such as crystal structure, crystallinity and film purity, may be changed or adjusted by the selection and combination of the particular precursor and co-reactant(s) which can alter the deposited film's electronic properties. ALD, as a deposition technique, is of particular interest as it can be performed sequentially, allowing for the production of high-quality, uniform and conformal films with targeted composition and thickness control, thanks to its inherent, self-limiting mechanism. ALD is performed by delivering a precursor in its vapor phase to a substrate surface where it then chemisorbs. The precursor in excess is then purged from the system after each subcycle. This subcycle of flow-purge is then repeated with any other reactants before another cycle of precursor addition. To achieve an ideal ALD process, a suitable organometallic compound is required. Generally, a precursor should possess good thermal stability to enable continuous and constant vaporization from source to deposition without decomposing. This is a minimum requirement in order to achieve a chemically driven, self-saturated growth regime across a wide temperature window; meanwhile, insufficiently stable precursors typically result in non-conformal deposition. An ideal precursor must also contain highly reactive chemical bonds to afford high growth per cycle (GPC), which is expected on a commercial scale. Finally, the precursor must have optimal physical properties that make it practical for high-volume manufacturing. This typically means being liquid at or near room temperature, which allows for the easier and more consistent transfer of bulk quantities into containers, and ideally delivering approximately 1 Torr vapor pressure significantly below 180 °C.

A wide variety of ALD rare earth precursor complexes have been previously reported; *β*-diketonates [18–20], silylamides [21,22], cyclopentadienyls [23–26], amidinates [27,28], guanidinates [29–33] and pyrazolates [34], to name a few examples. *β*-diketonates, such as *tris*(2,2,6,6-tetramethyl-3,5-heptanedionate)yttrium, Y(thd)$_3$ [18], and *tris*(2,7,7-trimethyl-3,5-octanedionate)yttrium, Y(fod)$_3$ [20], were among the first examples to be assessed; these compounds typically exhibit undesirably high melting points (generally exceeding 150 °C). Their primary advantage is superior thermal stability, but at the cost of low vapor pressure. Furthermore, they often suffer from high bulkiness and poor reactivity with oxidants, which results in low GPC and the need for high deposition temperatures [35] or plasma enhanced methods [36]. In addition, while they may have similar thermodynamic vapor pressures compared with liquid precursors, they are still limited by slower evaporation kinetics. For this reason, liquid precursors are typically preferred for ALD processes. Silylamides, such as *tris*(*N*,*N'*-*bis*(trimethylsilyl)amido)yttrium, Y(tmsa)$_3$, have sufficient stability and volatility, but when applied in modern techniques regularly lead to silicon incorporation [22]. Thus, silicon-free options are also desirable, such as cyclopentadienyls and amidinates, which will be discussed in detail later in this paper. In this work, we report the design and preparation of novel heteroleptic rare earth compounds which possess melting points at or below room temperature, specifically exemplified by the yttrium complex, Y(EtCp)$_2$(^{i}Pr$_2$-amd). The ALD of Y_2O_3 films illustrate the use of such a liquid pre-

cursor in combination with ozone, oxygen and water. The ALD process conditions that are required to deposit Y_2O_3 films were developed to optimize the composition, morphology, uniformity, conformality and the crystallinity of the resulting films. The obtained films were also investigated for plasma etch resistance and hydrophobicity applications.

2. Experimental Section

2.1. General Analysis

^{1}H and ^{13}C nuclear magnetic resonance (NMR) spectra were measured on a Bruker AVANCE NEO 400 spectrometer (Billerica, MA, USA) at 298 K. All signals were referenced to the residual proton signals of deuterated solvents and corrected to the tetramethylsilane (TMS) standard values. The melting point of all compounds was analyzed by differential scanning calorimetry (DSC, Bruker DSC3100SA). Volatility and thermal stability were analyzed in the range of 25–500 °C (heating ramp of 10 °C/min; N_2 gas flow: 220 sccm) at atmospheric pressure by thermogravimetric analysis (Mettler Toledo TGA/DSC 3+) using a typical sample size of 20–25 mg in an aluminum crucible. Alternative TGA experiments were run at a reduced pressure of 10–20 Torr and closed cup experiments using an aluminum crucible sealed by a perforated cap with a hole of 0.1 mm diameter.

2.2. General Conditions for Inert Reactions

All compounds were highly sensitive to moisture and oxygen. Solvents were dried by a solvent purification system (MBraun). The handling and syntheses of all air and moisture-sensitive compounds were carried out under argon atmosphere using standard Schlenk techniques. All chemicals and reagents used were commercially acquired, unless otherwise stated. All mentions of YCl_3 were in the form of an anhydrous salt.

Li-^{i}Pr$_2$-amd 1 equivalent of diisopropylcarbodiimide was added into dry THF under an inert atmosphere. The solution was cooled to −78 °C by a dry ice bath followed by the dropwise addition of 1.1 equivalents of MeLi (1.6 M in diethyl ether) via a dropping funnel over a period of 30 min. The resulting yellowish solution was brought to r.t. and stirred for a further 2 h.

LiRCp (R = Me, Et, ^{i}Pr) was prepared by cracking a corresponding dicyclopentadiene derivative at 200 °C under inert atmosphere, purified via distillation and collected at −78 °C. The relevant Cp derivative was then dissolved in dry THF under N_2 and deprotonated with ^{n}BuLi and allowed to reach r.t. over 3 h. Obtained Li-RCp solution was typically 1–2 M.

2.3. General Procedure For Preparation of Y(RCp)$_2$(^{i}Pr$_2$-amd) (R = Me, Et, ^{i}Pr)

YCl_3 was stirred in dry THF at r.t. The reaction was then cooled to −78 °C followed by slow addition of 2 equivalents of Li-RCp (R = Me, Et, ^{i}Pr) and allowed to reach r.t. before being stirred for a further 12 h to produce Y(RCp)$_2$Cl, without isolation. The solution was once more cooled to −78 °C, followed by the slow addition of 1 equivalent of the aforementioned Li-^{i}Pr$_2$-amd solution. The solution was allowed to reach r.t. and stirred for a further 12 h. The mixture was evaporated to dryness under vacuum and followed by re-dissolving either into pentane or toluene. Pentane or toluene was then isolated by filtration. The solvent was evaporated to dryness under vacuum to obtain a pale-yellow oil, or waxy solid. Purification was carried out either by sublimation or via short-path distillation.

Y(MeCp)$_2$(^{i}Pr$_2$-amd), the yellow waxy solid, was sublimed at 115 °C at 14 mTorr. Yield was 67.8%, m.p. 26.1 °C. ^{1}H NMR (C_6D_6, 400 MHz): δ 0.95 (*d*, 12H, $^3J_{HH}$ = 8.0 Hz, Y-NCH*Me*$_2$), 1.50 (*s*, 3H, Y-N$_2$C*Me*), 2.14 (*s*, 6H, Y-Cp*Me*), 3.28 (*m*, 2H, Y-NC*H*Me$_2$), 5.98−6.11 (*m*, 8H, Y-*Cp*Me).

Y(EtCp)$_2$(^{i}Pr$_2$-amd) purification was carried out using a short-path distillation column at a temperature of 90−120 °C, at 20 mTorr. Yield was 45.7%, m.p. 5.7 °C. ^{1}H NMR (C_6D_6, 400 MHz): δ 0.96 (*d*, 12H, $^3J_{HH}$ = 4.0 Hz, Y-NCH*Me*$_2$), 1.22 (*t*, 6H, $^3J_{HH}$ = 4.0 Hz, Y-CpCH$_2$C*H*$_3$), 1.51 (*s*, 3H, Y-N$_2$C*Me*), 2.54 (*q*, 4H, $^3J_{HH}$ = 4.0 Hz, Y-CpC*H*$_2$CH$_3$), 3.29 (*m*, 2H, Y-NC*H*Me$_2$), 6.04−6.11 (*m*, 6H, Y-*Cp*Me).

Y(^{i}PrCp)$_2$(^{i}Pr$_2$-amd) purification was carried out by short-path distillation at 120−150 °C at 20 mTorr. Yield was 76%. ^{1}H NMR (C$_6$D$_6$, 400 MHz): δ 0.98 (*d*, 12H, $^3J_{HH}$ = 8.0 Hz, Y-NCH*Me*$_2$), 1.26 (*d*, 12H, $^3J_{HH}$ = 4.0 Hz, Y-CpCH*Me*$_2$), 1.51 (*s*, 3H, Y-N$_2$C*Me*), 2.14 (*s*, 6H, Y-Cp*Me*), 2.92 (*m*, 2H, Y-NC*H*Me$_2$), 3.30 (*m*, 2H, Y-CpC*H*Me$_2$), 6.10−6.13 (*m*, 8H, Y-*Cp*CHMe$_2$).

2.4. Y$_2$O$_3$ Film Analysis

Y$_2$O$_3$ thin film thicknesses and refractive indexes were routinely measured using a spectroscopic ellipsometer (SEMILAB, SE-2000, Budapest, Hungary) with a wavelength from 245 to 1000 nm. The corresponding surface and in-depth film compositions were determined by X-ray photoelectron spectroscopy (XPS) using Al Kα (λ = 0.834 nm) X-rays generated at 15 kV and 70 W (Thermo Fisher Scientific, K-alpha, Waltham, MA, USA). Surface morphology was characterized by atomic force scanning electron microscopy (SEM, Hitachi High-tech, S-5000, Tokyo, Japan) and atomic force microscopy (AFM, Asylum Research MFP-3D, Santa Barbara, CA, USA) in tapping mode. Fourier transform infrared spectroscopy (FTIR, Thermo Scientific, Nicolet iS-50, Waltham, MA, USA), performed in a 600−4000 cm^{-1} spectral range, was used to detect surface chemical functional groups. The data were collected from 600 to 4000 cm^{-1} with a resolution of 4 cm^{-1}. XRD patterns were acquired on Rigaku SmartLab diffractometers (Rigaku, Tokyo, Japan) using Cu Kα radiation (λ = 0.154 nm).

2.5. ALD of Y$_2$O$_3$ Films

Yttrium oxide films discussed in this paper were grown on HF-cleaned silicon substrates either in a 150 mm Atomic-Premium CN-1, a Beneq TF-200 reactor or in home-built tubular ALD systems. During the development of the Y$_2$O$_3$ ALD process, Y(EtCp)$_2$(^{i}Pr$_2$-amd) was selected as the yttrium precursor, due to its superior volatility, stability and melting point (liquid at 6 °C). Water and ozone were assessed as oxygen sources. The precursor was held in a stainless-steel bubbler at 95 °C for optimal vapor pressure, and the delivery line was maintained slightly above, at 120 °C, to prevent precursor condensation. Nitrogen was used as a purge gas, and was introduced in the precursor bubbler through a dip-tube for effectively carrying regular flow rates of the precursor vapors to the ALD chamber. Water was kept at room temperature, and the delivery line was heated to 35 °C. The as-deposited ALD yttrium oxide films were used as such, or annealed in vacuo in a furnace from 600 °C for 4 min in a flow of 35 cc of nitrogen.

2.6. ICP Plasma-Etching Experiments

Y$_2$O$_3$ and other representative thin films, each deposited on silicon substrates, were introduced into an inductively coupled plasma (ICP) etcher tool (200 mm Alcatel MS100). The erosion behaviors of such protective coatings were analyzed under the plasma etching conditions using the same bias power and processing gases (CF$_4$ and O$_2$) where high-density CF$_4$/O$_2$ plasma are produced (RF source power: 1300 W. RF bias power: 200 W. Chamber pressure: 1.1 Pa. CF$_4$:O$_2$ flow rates: 30:5 sccm. Etching time: up to 4 min). Y$_2$O$_3$ tested here was deposited by ALD as described in the corresponding section below. For comparison, different relevant materials were tested: 200 nm-thick PECVD SiO$_2$ and 100 nm-thick LPCVD SiO$_2$ films were obtained from Advantec and SUMCO, respectively; 300 nm-thick SiN LPCVD samples were provided by Advantec; 550 nm-thick Y$_2$O$_3$ ALD and 500 nm-thick Al$_2$O$_3$ ALD films were obtained from Beneq; 35 nm-thick YF$_3$ ALD was prepared internally, using a process that will be described separately.

2.7. Water Contact Angle (WCA) Measurements

The Y$_2$O$_3$ ALD films, used for hydrophobic tests, were prepared using Y(EtCp)$_2$(^{i}Pr$_2$-amd) and O$_3$ at 200 °C. Water contact angles were measured by the water drop technique using a contact-angle analyzer (Excimer, Simage AUTO 100, Tokyo, Japan) with deionized water (1.8 × 10^5 Ohm at 20 °C). Contact angle pictures were obtained by a charge-coupled device video camera and drop shape analysis software. The volume of each deionized water droplet used was 5 μL.

3. Results and Discussion

3.1. Y_2O_3 ALD Precursor Selection

In previous studies, thermal- and plasma-enhanced ALD of Y_2O_3 have both been investigated using several known derivatives of cyclopentadienyl (Cp) yttrium precursors, with YCp_3 and $Y(MeCp)_3$ receiving the most interest. Generally, yttrium cyclopentadienyl compounds are solid at room temperature and have moderate vapor pressures; however, they do display high GPC, typically exceeding well beyond 1 Å/cycle. They quickly react with water [23–26], O_2 plasma, [34] and O_3 [7]. Another common compound, $Y(^iPr_2\text{-amd})_3$, is part of the yttrium amidinate family of precursors, which are also solid at room temperature; have relatively low volatility; and deliver comparatively lower GPC, generally below 1 Å [27].

A promising approach to improving physical properties lies in targeting stable heteroleptic precursors, a strategy that can deliver considerable benefits over their homoleptic counterparts. This concept was first introduced in the late 2000 s and has since then gained tremendous attention, resulting in significant ALD process improvements [25].

In order to overcome the physical limitations of the $Y(RCp)_3$ and $Y(R\text{-amd})_3$ families, we applied this approach by investigating a series of yttrium heteroleptic compounds containing a combination of diisopropyl amidinate ($^iPr_2$-amd) and cyclopentadienyl derived ligands, which separately have shown varied success in ALD and CVD processes. Our study primarily focused on the preparation and deposition of $Y(RCp)_2(^iPr_2\text{-amd})$ compounds (R = Me, Et, ^iPr), consisting of cyclopentadienyl and amidinate ligands bonded to the same yttrium core. To the best of our knowledge, they are the only yttrium precursors reported to be liquid at room temperature to date, making them highly interesting for Y_2O_3 ALD at an industrial scale.

The preparation of the target compounds was generally conducted by reacting two equivalents of Li-RCp with YCl_3 followed by one equivalent of Li-$^iPr_2$-amd and purified via vacuum distillation, or sublimation. Each compound was assessed by thermogravimetric analysis (TGA) using approximately 20 mg of $Y(MeCp)_3$, $Y(EtCp)_3$, $Y(MeCp)_2(^iPr_2\text{-amd})$, $Y(EtCp)_2(^iPr_2\text{-amd})$ and $Y(^iPr_2\text{-amd})_3$, in order to compare their volatility and stability. Initial tests suggested excellent evaporation behavior for the heteroleptic compounds, as illustrated in Figure 1. A comparison between the vapor pressures of $Y(MeCp)_3$, $Y(MeCp)_2(^iPr_2$-amd) and $Y(EtCp)_2(^iPr_2$-amd) is shown in Figure 2 for the low-temperature domain. All data were acquired by the TGA isotherm method [37,38] under standard operating temperatures used to vaporize ALD precursors. These results indicate that $Y(EtCp)_2(^iPr_2\text{-amd})$ possesses superior volatility in the low-temperature region, with a partial pressure of 1 Torr at 150 °C. Table 1 summarizes the most relevant physical properties of the complexes $Y(RCp)_3$, $Y(^iPr_2$-amd)$_3$ and $Y(RCp)_2(^iPr_2$-amd). Remarkably, all heteroleptic compounds prepared showed significantly lower melting points than either of their homoleptic counterparts.
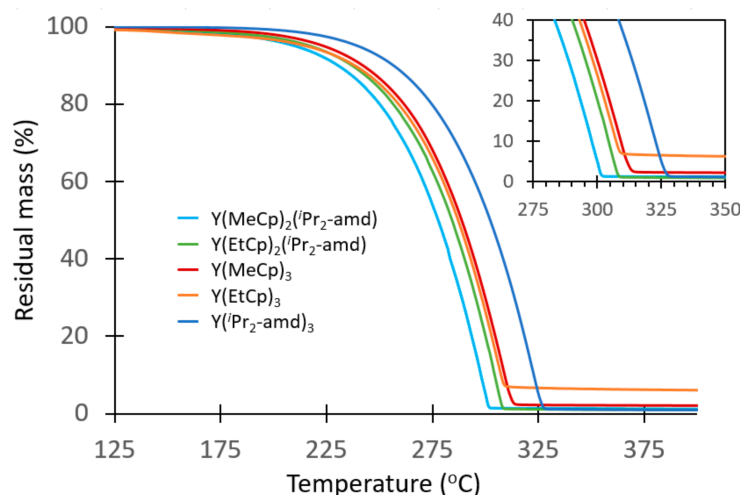
Figure 1. TGA comparison of yttrium precursors.
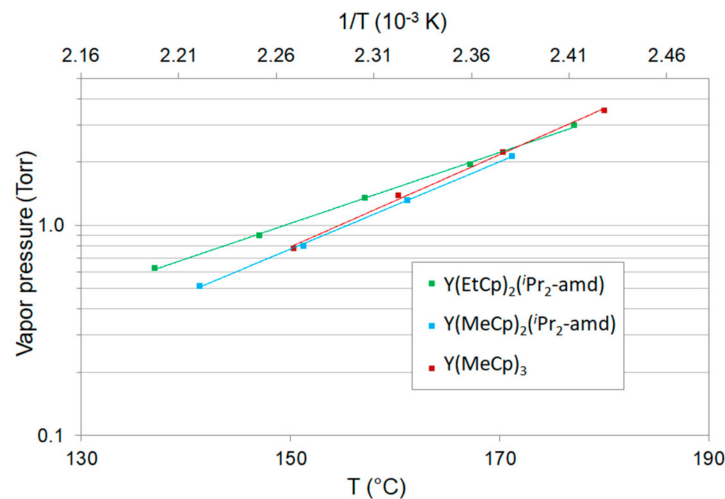
Figure 2. Vapor pressure comparison of selected yttrium precursors $Y(EtCp)_2(^iPr_2\text{-amd})$ [$R^2 = 0.9988$], $Y(MeCp)_2(^iPr_2\text{-amd})$ [$R^2 = 0.9991$] and $Y(MeCp)_3$ [$R^2 = 0.9974$].

Table 1. Thermal properties of homoleptic $Y(RCp)_3$ and $Y(^iPr_2\text{-amd})_3$ vs. heteroleptic $Y(RCp)_2(^iPr_2\text{-amd})$ compounds.

Y Precursor	Molecular Weight (g/mol)	Melting Point * (°C)	Temperature for VP = 1 Torr ** (°C)
$Y(MeCp)_3$	326.27	124	155
$Y(EtCp)_3$	368.34	60	200
$Y(^iPrCp)_3$	410.51	55	> 200
$Y(^iPr_2\text{-amd})_3$	514.03	175	201 [29]
$Y(MeCp)_2(^iPr_2\text{-amd})$	388.50	26	155
$Y(EtCp)_2(^iPr_2\text{-amd})$	416.55	6	150
$Y(^iPrCp)_2(^iPr_2\text{-amd})$	444.60	Liquid at R.T.	168

* measured by DSC; ** measured by isotherm method.

The rest of this study focuses on the $Y(EtCp)_2(^iPr_2\text{-amd})$ precursor, which we concluded to possess the most suitable physical properties, as it is liquid well below room temperature and delivers the highest volatility in the low-temperature region.

In order for an ALD precursor to be deemed a viable candidate, its long-term thermal stability must also be assessed to ensure consistent performance over an extended period of use. This was of particularly critical importance as some heteroleptic complexes have been reported to undergo ligand exchange reactions [39]. To ensure its long-term stability, the $Y(EtCp)_2(^iPr_2\text{-amd})$ precursor was subjected to a series of thermal stress tests. The compound was placed in an airtight vessel and continuously heated, with periodic analysis, so as to observe any chemical changes. $Y(EtCp)_2(^iPr_2\text{-amd})$ was heated over a 4-week period at 120 °C and monitored via ^{1}H NMR every 2 weeks; these conditions were intended to reflect the delivery conditions of the precursor as closely as possible. A comparison of the ^{1}H NMR spectra taken during the study can be seen in Figure 3: no appearance of detectable free-ligand, or conversion to homoleptic compounds, $Y(EtCp)_3$ and $Y(^iPr_2\text{-amd})_3$, was observed. A separate measurement by TGA also supports the absence of changes in the compound's physical properties beyond a reasonable margin of error. These initial results indicated that the precursor was sufficiently stable for ALD testing.
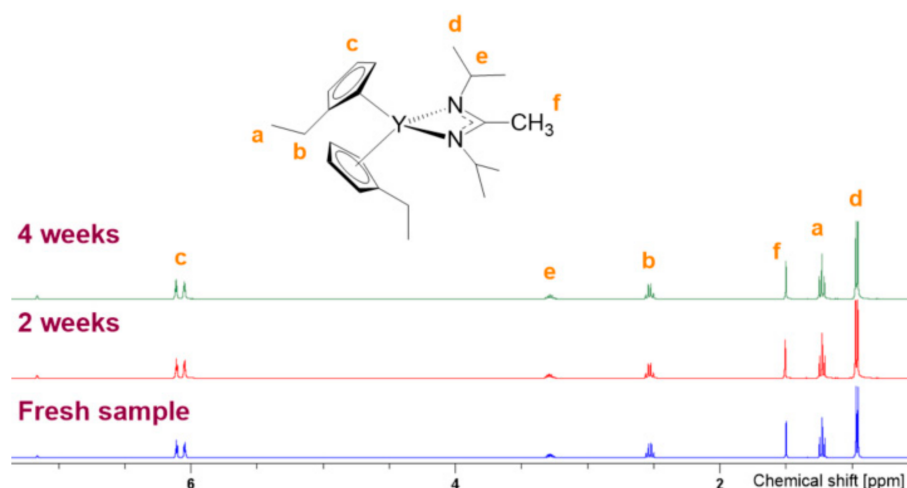
Figure 3. ^{1}H NMR of Y(EtCp)$_2$(^{i}Pr$_2$-amd) before and during 120 °C thermal stability test.

3.2. Y$_2$O$_3$ ALD Process Characterization

The ALD evaluation of Y(EtCp)$_2$(^{i}Pr$_2$-amd) with various oxidants, such as ozone, water and oxygen, was performed on bare 150 mm Si substrates. Initial tests with ozone were carried out at 300 °C while increasing source introduction time from 5 up to 25 s (shown in Figure 4 below). From 10 to 25 s, the GPC was found to remain close to $1-1.1$ Å/cycle, with the deposited films also displaying excellent uniformity (N.U. < 3%). This experiment suggests that the precursor is capable of depositing via a self-limiting mechanism, consistent with expected ALD behavior, with each of the co-reactants (Figure 4).
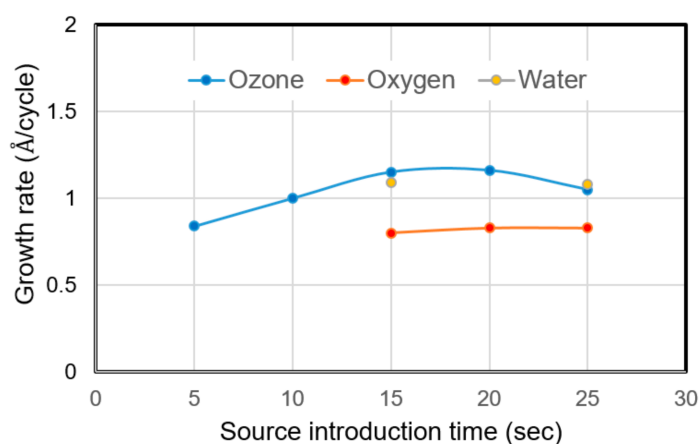

Figure 4. Growth rate as a function of source introduction time at 300 °C using O$_3$, H$_2$O and O$_2$ as co-reactant.

Based on optimized process conditions, the ALD window for Y(EtCp)$_2$(^{i}Pr$_2$-amd) was determined to be between 300 and 450 °C, using ozone as the co-reactant. Under these conditions, a GPC of $0.9-1$ Å and non-uniformity of less than 5 % on a 150 mm wafer was achieved (Figure 5). Deposited films were stoichiometric with a Y:O ratio of about 40:60, as observed by XPS, with negligible carbon and nitrogen impurities. The refractive index values ranged from 1.9 to 2.0.
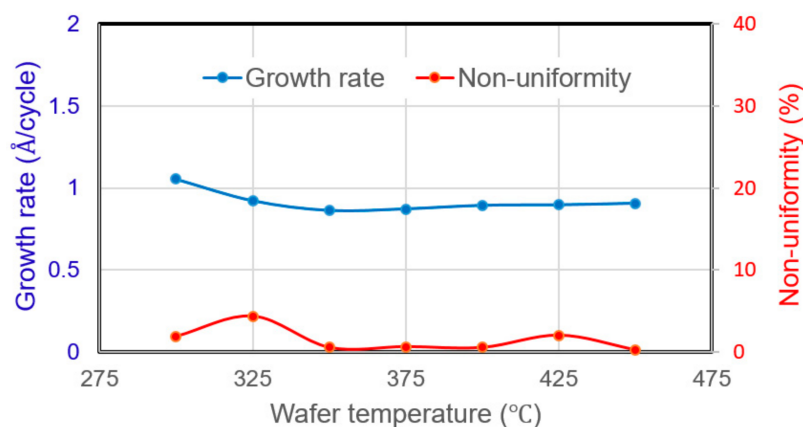
Figure 5. ALD window of Y(EtCp)$_2$(^{i}Pr$_2$-amd) and ozone.

Water as the co-reactant was found to require similar process conditions as established for ozone with the ALD window being similarly observed from 300 to 450 °C. GPC reached 0.9 Å (Figure 4), and non-uniformity was less than 5 %. The refractive index values also ranged from 1.9 to 2.0, in line with the value observed for other films deposited by ALD. A notable difference in behavior was observed by altering water pressure, which was found to affect GPC. When low partial pressure (<0.1 Torr) was employed, the GPC was shown to continuously increase as a function of wafer temperature up to 450 °C, whereas with higher partial pressure (>0.2 Torr), a constant GPC was observed across the same temperature range. This suggests that high partial water pressure is required in order to achieve a complete reaction at the surface during the water pulse. This was attributed to lower reactivity between Y(EtCp)$_2$(^{i}Pr$_2$-amd) and water, compared with ozone. This may imply that a self-limited reaction is incomplete or imperfect at low partial pressure. Alternatively, the observations may be explained by an unfavorable adsorption/desorption equilibrium at low partial pressure of water, resulting in an incomplete oxidation of the ligands.

It is worth noting that Y(EtCp)$_2$(^{i}Pr$_2$-amd) also performed comparably well with O$_2$ as a co-reactant in thermal mode. The ALD window closely matched those of ozone and water, 300 to 450 °C. The GPC fell into the range of 0.8−0.9 Å, similar to the other known processes, and non-uniformity was shown to be less than 5 % in 150 mm wafer; these data indicate a similar outcome to the earlier results. The refractive index values also ranged from 1.9 to 2.0, suggesting comparable film quality. It was noticed by XPS analysis that altering oxygen pulse times ultimately changed the level of impurities in the final film, especially for films deposited at 300 °C. Furthermore, 1 s of O$_2$ resulted in a high carbon impurity of 5−6 at. %. If the pulse time was extended to 20 s, the percentage of carbon impurity was found to fall below the detection limit. As observed with water, high partial pressure, or long introduction time of oxygen, was shown to play an important role in achieving complete reaction and depositing high-purity films.

Figure 6 shows the X-ray diffraction (XRD) pattern of an 8−10 nm Y$_2$O$_3$ film deposited by Y(EtCp)$_2$(^{i}Pr$_2$-amd) and ozone from 250 to 400 °C under optimized conditions. Amorphous films were observed at 250 °C. The films became polycrystalline as the wafer deposition temperatures were increased, which was indicated by stronger peaks in the XRD patterns from 300 °C.

Scanning electron microscopy (SEM) was used to measure step coverage of a 1:20 aspect ratio structure deposited at 300 °C. The SEM image (Figure 7) shows that excellent step coverage was obtained (top: 42 nm/bottom: 40 nm), opening interesting perspectives for industrial applications requiring high conformality.
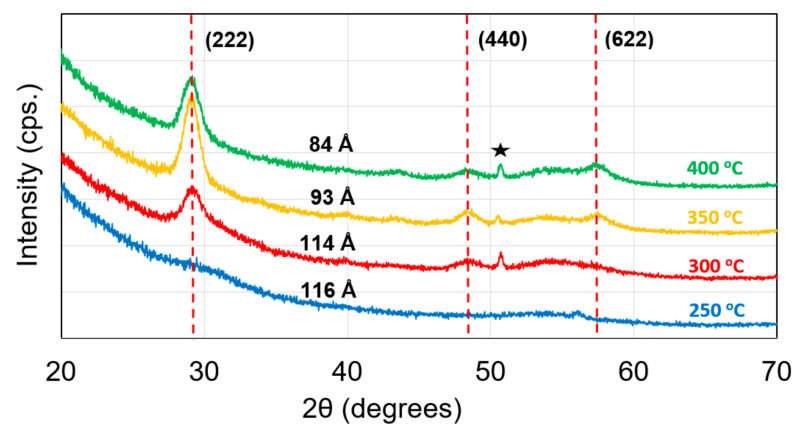
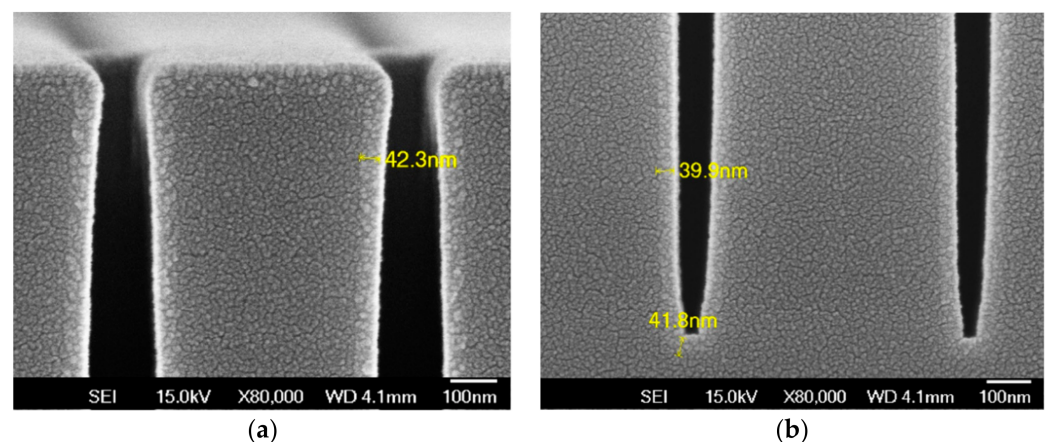**Figure 6.** XRD of Y_2O_3 films deposited by Y(EtCp)$_2$(^{i}Pr$_2$-amd) and ozone (★ by silicon substrate).

(**a**)   (**b**)

Figure 7. SEM images of a Y_2O_3 film grown by Y(EtCp)$_2$(^{i}Pr$_2$-amd) and O$_3$ into a deep trench with aspect ratio 1:20: (**a**) top of trench; (**b**) bottom of trench.

3.3. Y_2O_3 ALD Layers as Anticorrosion Protective Coatings

In the first set of experiments, Y_2O_3 coupons were introduced in an inductively coupled plasma (ICP) etch reactor together with silicon oxide and silicon nitride samples. Experiments were carried out using a low-pressure CF$_4$/O$_2$-based plasma. As shown in Figure 8, both thermal and PECVD silicon oxide films were etched out after less than 2 min of process time, with the silicon nitride film eroding at an even greater rate. By comparison, the erosion rate of Y_2O_3 remained moderate after 4 min. This observed fast etch rate of silicon-based materials is consistent with earlier reports by Riley et al. [40].

A second set of erosion tests involved Y_2O_3, YF$_3$ and Al$_2$O$_3$ films, prepared by ALD either by Air Liquide (AL) or provided by Beneq Oy. Based on Table 2, alumina was found to be etched at least one order of magnitude faster than the yttrium-containing materials. Of these, YF$_3$ was found to be eroded at a marginally faster rate than Y_2O_3. Importantly, the etching experiment found erosion rates to be nearly identical between the two, as well as very similar for both ultra-thin Y_2O_3 (35 nm, deposited at AL) and thin Y_2O_3 (550 nm, deposited at Beneq Oy). Although the reproducibility seems very good for each type of material, a further study needs to be conducted to determine if this is a consistent feature, or for instance if films deposited under altered conditions will display different behavior. The significantly higher performance of Y_2O_3 vs. Al$_2$O$_3$, with a ratio of etch rates > 12, should be noted and is consistent with literature values [40].
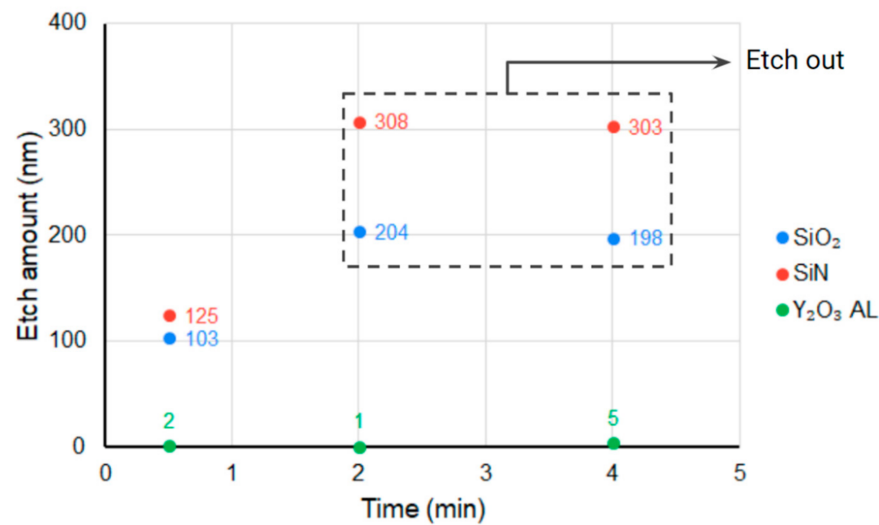
Figure 8. Etch of silica, silicon nitride and yttrium oxide thin films vs. process time.

Table 2. Etch rates of Y_2O_3, YF_3 and Al_2O_3 ALD thin films. The films were either atomic layer deposited internally, or provided by Beneq.

Y Film	Etch Rate (nm/min)	ALD Film Thickness (nm)
Y_2O_3 AL	1.04	35
Y_2O_3 Beneq	1.10	550
YF_3 AL	1.85	35
YF_3 Beneq	13.53	500

Some mechanistic insight may be gained from the provided XPS spectra (Figure 9) While the film was originally stoichiometric, with no detected impurities, plasma etching after 4 min revealed the surface to be rich in fluorine. F-contamination was also observed deeper into the bulk of the film. This may suggest that the abrasion mechanism consists of two steps: (1) fluorination of the Y_2O_3 at the surface, proceeded by (2) removal of the material in the form of a fluoride or an oxyfluoride. Such modification of the Y_2O_3 surface to the YO_xF_y surface after the first fluorine radical exposure was already reported [12] and suggests studying YF_3 as an alternative protective ALD layer.


(**a**)   (**b**)
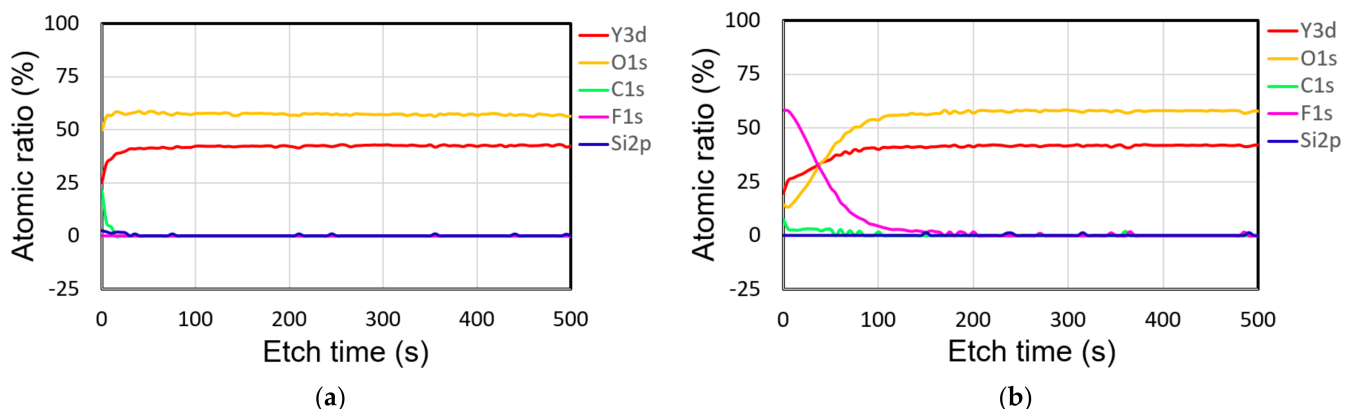
Figure 9. In-depth XPS analyses of as-deposited (**a**) and plasma etched (**b**) Y_2O_3 films.

3.4. Y_2O_3 ALD Layers as Hydrophobic Coatings

Azimi et al. reported that rare earth oxide thin films deposited by PVD are hydrophobic [41], which was proposed to be a property derived from the unfilled 4f orbitals being shielded by the $5s^2$ and $5p^6$ electrons, though this conclusion was subject to controversy [42].

This approach was extended to materials deposited via ALD by Oh et al. [43] where the authors observed water contact angles (WCA) ranging between 90° and 105° for flat surfaces, and even demonstrated superhydrophobic behavior (WCA > 135°) on textured surfaces. The paper also reported that both Y_2O_3 and La_2O_3 (among other rare earth oxides) exhibit similar hydrophobic properties. However, their electronic orbital configurations differ, meaning the "$5s^2p^6$ orbital shielding effect" described for lanthanum oxide cannot be applied to yttrium oxide. This section attempts to elucidate the underlying causes of the hydrophobicity observed in rare earth oxide materials.

In order to compare the hydrophobic character across a range of materials, our study considered the following films for WCA testing: Y_2O_3; La_2O_3 (trivalent rare earth oxides); ZrO_2; HfO_2 (group IV oxides); and finally, Nb_2O_5 and Ta_2O_5 (group V oxides). Each was deposited by ALD and exposed to an open-atmosphere for a period of at least one month prior to analysis. Our study concluded that a WCA of over 90° could indeed be observed in our rare earth oxide deposits before annealing (bottom left picture of Figure 10), after weeks of air exposure. For comparison, the thin films of non-rare earth oxides generally displayed a WCA of $60-80°$, while 30° can be typically expected for silica or untreated silicon wafers. All films were then subjected to annealing at 600 °C for 4 min (N_2 flow rate: 30 sccm, reactor pressure < 0.1 Torr). In each case, lower WCAs were observed when measured immediately after annealing, reaching down to about 10° for rare earth oxides vs. about $30-45°$ for non-rare earth films. After annealing, WCAs gradually recovered their original values within approximately one week (as illustrated Figure 10 for Y_2O_3). Subsequent annealing tests with either similar or different conditions provided roughly the same trends. Finally, dedicated thin films of yttrium oxide were deposited, immediately followed by WCA measurements. Films were found to be initially very hydrophilic (WCA < 10°), with WCAs rising over time, confirming the previous observations after annealing. These results indicate that the electronic configurations of the oxides seem unrelated to the observed hydrophobicity seen in rare earth oxides, and that reported hydrophobic properties are not inherent to the film's bulk electronic configuration, but rather to its surface state.
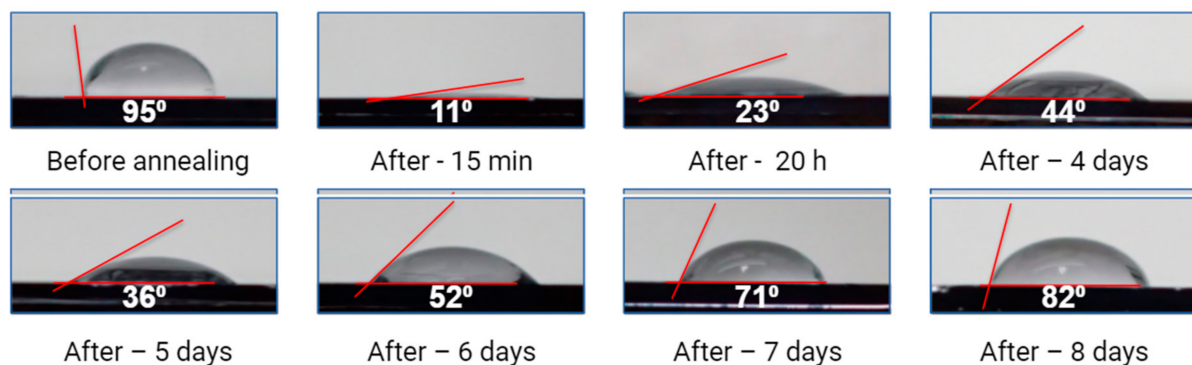
Figure 10. WCAs on Y_2O_3 before and after different duration of air exposure.

Alternative hypotheses were proposed: (1) a possible roughness change due to the hygroscopic nature of rare earth materials; (2) thickness dependence and a possible correlated change in surface free energy [43]; (3) adsorption of ambient hydrocarbons [44–47].

In order to address the first hypothesis, AFM analysis was carried out on each sample available to assess the film roughness. The root mean square (RMS) values were typically near 100 pm and were never observed to exceed 260 pm (Figure 11). Each film had a relatively smooth surface both before and after annealing, as well as upon aging. No short-range or long-range microstructure was observed. Thus, we feel it can be concluded that roughness is unlikely to play a significant role in the observed phenomena.
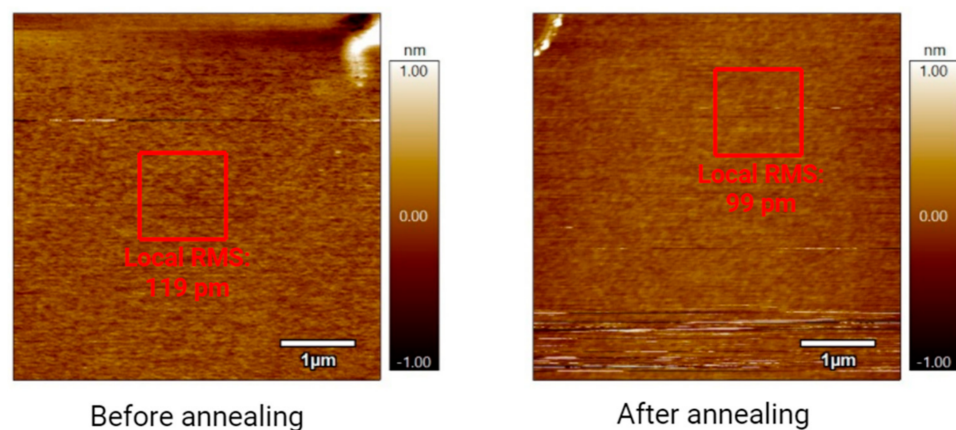
Figure 11. AFM analyses of Y_2O_3 films before and after annealing.

Different depositions were then performed to assess a possible influence of the thickness on WCA. We compared the WCAs of annealed films of Y_2O_3 for thicknesses ranging from 12 to 34 nm on silicon or silica substrates. WCAs were found to fall in the $60-95°$ range. No significant difference was observed at constant thickness and time after annealing. As observed earlier, the WCA was found to increase with extended exposure to the open atmosphere. The study by Zhao et al. [44] revealed that the surface free energy is inversely proportional to the thickness of the material, where thinner films resulted in a lower WCA. Thus, films significantly below 20 nm are associated with a WCA of 90° or less. This inverse relationship was also observed in our deposited films, consistent with the findings of that report. However, it is likely that another phenomenon is working in tandem with this surface free energy/thickness observation.

The possible influence of atmospheric organic species on the WCA was finally examined. While no impurities were observed in the bulk of the film by XPS, carbon was expectedly observed in the surface of the films. WCA seems to also correlate with C content observed at the surface, as could be seen in our samples: 25° for 9%, C content, 37° for 18% and 61° for 25%, respectively.

Such observations needed to be complemented with a more systematic approach. Annealed Y_2O_3 samples of about 10 to 30 nm were initially checked to confirm their hydrophilic character (WCA ~11°) before exposure to an open-atmosphere or introduced in an enclosure containing a flask filled with toluene. A valve between the enclosure and a pump was opened allowing for gases to be purged, and closed once more, allowing the N_2 atmosphere to become saturated with toluene. Y_2O_3 was then allowed to remain exposed to toluene vapors for periods of 6 to 24 h (Figure 12) The enclosure was purged prior to sample withdrawal. WCAs were then measured and compared with ambient atmosphere exposed Y_2O_3 films. A difference in WCA was observed between the two conditions, which increased further with extended experiment duration: 24° after 6 h, 29° after 8 h and 40° after 24 h (Table 3). The results of this experiment indicate that the intentional exposure of toluene leads to a dramatic increase in WCAs vs. unexposed films. This leads us to the conclusion that carbon incorporation into the surface of Y_2O_3 materials significantly contributes to its hydrophobic character, which can be observed after long periods of atmospheric exposure.
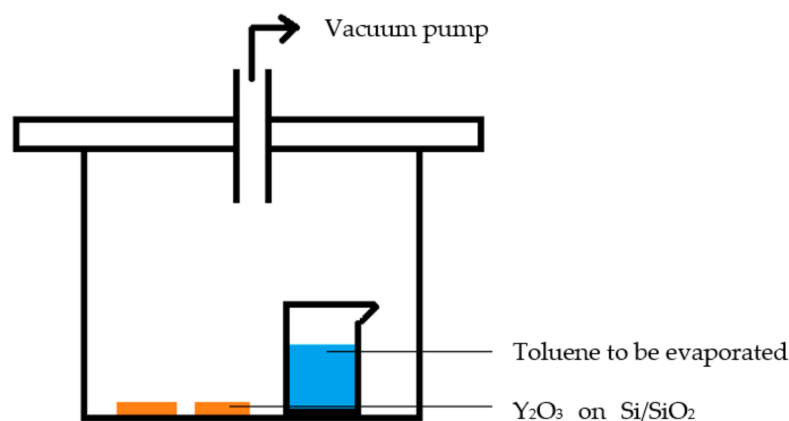
Figure 12. Enclosure where Y_2O_3 films are exposed to toluene vapors, after being vacuumed.

Table 3. WCA evolution of Y_2O_3 ALD film before, immediately after annealing and over time.

Experimental Conditions	Before Annealing	Right After Annealing	6 h	8 h	24 h
In nitrogen, with hydrocarbon exposure	86°	41°	69°	71°	87°
In air, without hydrocarbon exposure	91°	39°	45°	42°	47°

4. Conclusions

There are a considerable number of applications for yttrium oxide thin films across various industries. Liquid, volatile and stable yttrium precursors are critical both to ensure the stable delivery of their vapors into deposition reactors and to obtain an industrially scalable process. It is also of vital importance that a compound results in a high GPC, which will enable high productivity. As reviewed in this paper, existing precursors suffer from at least one drawback, typically having a high melting point, insufficient thermal stability and/or low GPC. The design of yttrium molecules combining the features of two complementary moieties (cyclopentadienyl and amidinates) led to the identification of an optimal heteroleptic compound, $Y(EtCp)_2(^iPr_2\text{-amd})$, a liquid at room temperature, which leads to a GPC of up to 1.1 Å in a process window ranging from 300 to 450 °C. The compound is reactive to O_3, H_2O and even O_2, although the latter requires longer oxidant pulses and/or higher partial pressure to completely remove impurities. O_3-based films appear smooth and crystalline, yielding the highest quality films of the three co-reactants with the shortest pulse times.

The films showed strong resistance to fluorine-containing plasma, outperforming other etch-resistant materials, such as silicon oxide, silicon nitride and alumina, behaving comparably to yttrium fluoride. Such described Y_2O_3 ALD films are thus promising candidates for potential applications in the field of anticorrosive coatings. The hydrophilic character initially exhibited by the rare earth oxide films turns hydrophobic after prolonged exposure to air or intentional organic exposure, which can be reversed upon annealing under N_2 flow. These observations may be attributed to physisorption/adsorption of trace organic species from the atmosphere. Such hydrophobic materials may find various applications as water-repellent layers under ambient to moderate conditions.

Author Contributions: Conceptualization, W.N., C.D.; methodology, W.N., J.L.; validation, C.D., N.B.; formal analysis and investigation, T.T., S.K., N.G., and T.O.; writing—original draft preparation; C.D., N.B., W.N., J.G., and N.G.; writing—review and editing, C.D., N.B., and J.G. All authors have read and agreed to the published version of the manuscript.

Informed Consent Statement: Not applicable.

References

1. Fukabori, A.; Yanagida, T.; Pejchal, J.; Maeo, S.; Yokota, Y.; Yoshikawa, A.; Ikegami, T.; Moretti, F.; Kamada, K. Optical and scintillation characteristics of Y_2O_3 transparent ceramic. *J. Appl. Phys.* **2010**, *107*, 073501. [CrossRef]
2. Krankel, C. Rare-Earth-Doped Sesquioxides for Diode-Pumped High-Power Lasers in the 1-, 2-, and 3-μm Spectral Range. *IEEE J. Sel. Top. Quantum Electron.* **2015**, *21*, 250–262. [CrossRef]
3. Jollet, F.; Noguera, C.; Thromat, N.; Gautier, M.; Duraud, J.P. Electronic structure of yttrium oxide. *Phys. Rev. B* **1990**, *42*, 7587–7595. [CrossRef] [PubMed]
4. Manchanda, L.; Gurvitch, M. Yttrium oxide/silicon dioxide: A new dielectric structure for VLSI/ULSI circuits. *IEEE Electron. Device Lett.* **1988**, *9*, 180–182. [CrossRef]
5. Lin, K.C.; Juan, P.C.; Liu, C.H.; Wang, M.C.; Chou, C.H. Leakage current mechanism and effect of Y_2O_3 doped with Zr high-K gate dielectrics. *Microelectron. Reliab.* **2015**, *55*, 2198–2202. [CrossRef]
6. Leng, J.; Yu, Z.; Li, Y.; Zhang, D.; Liao, X.; Xue, W. Optical and electrical properties of Y_2O_3 thin films prepared by ion beam assisted deposition. *Appl. Surf. Sci.* **2010**, *256*, 5832–5836. [CrossRef]
7. Shim, J.H.; Chao, C.C.; Huang, H.; Prinz, F.B. Atomic layer deposition of yttria-stabilized zirconia for solid oxide fuel cells. *Chem. Mater.* **2007**, *19*, 3850–3854. [CrossRef]
8. Oh, S.; Park, J.; Shin, J.W.; Yang, B.C.; Zhang, J.; Jang, D.Y.; An, J. High performance low-temperature solid oxide fuel cells with atomic layer deposited-yttria stabilized zirconia embedded thin film electrolyte. *J. Mater. Chem. A* **2018**, *6*, 7401–7408. [CrossRef]
9. Iwasawa, J.; Nishimizu, R.; Tokita, M.; Kiyohara, M.; Uematsu, K. Plasma-resistant dense yttrium oxide film prepared by aerosol deposition process. *J. Am. Ceram. Soc.* **2007**, *90*, 2327–2332. [CrossRef]
10. Zavareh, M.A.; Sarhen, A.A.D.M.; Razak, B.B.; Basirun, W.J. Plasma thermal spray of ceramic oxide coating on carbon steel with enhanced wear and corrosion resistance for oil and gas applications. *Ceram. Int.* **2014**, *40*, 14267–14277. [CrossRef]
11. Kim, D.M.; Kim, K.B.; Yoon, S.Y.; Oh, S.Y.; Kim, H.T.; Lee, S.M. Effects of artificial pores and purity on the erosion behaviors of polycrystalline Al_2O_3 ceramics under fluorine plasma. *J. Ceram. Soc.* **2009**, *117*, 863–867. [CrossRef]
12. Lin, T.K.; Wang, W.K.; Huang, S.Y.; Tasi, C.T.; Wuu, D.S. Comparison of erosion behavior and particle contamination in mass-production CF_4/O_2 plasma chambers using Y_2O_3 and YF_3 protective coatings. *Nanomaterials* **2017**, *7*, 183. [CrossRef]
13. Shih, H. *Corrosion Resistance*; The Institute of Metals: London, UK, 1972; pp. 1–34. ISBN 978-953-51-0467-4.
14. Kim, D.M.; Lee, S.H.; Alexander, W.B.; Kim, K.B.; Oh, Y.S.; Lee, S.M. X-Ray Photoelectron Spectroscopy Study on the Interaction of Yttrium–Aluminum Oxide with Fluorine-Based Plasma. *J. Am. Ceram. Soc.* **2011**, *94*, 3455–3459. [CrossRef]
15. Qin, X.P.; Zhou, G.H.; Yang, H.; Wong, J.I.; Zhang, J.; Luo, D.W.; Wang, S.W.; Ma, J.; Tang, D.Y. Fabrication and plasma resistance properties of transparent YAG ceramics. *Ceram. Int.* **2012**, *38*, 2529–2535. [CrossRef]
16. Ruoho, M.; Niemelä, J.P.; Guerra-Nunez, C.; Tarasiuk, N.; Robertson, G.; Taylor, A.A.; Maeder, X.; Kapusta, C.; Michler, J.; Utke, I. Thin-Film Engineering of Mechanical Fragmentation Properties of Atomic-Layer-Deposited Metal Oxides. *Nanomaterials* **2020**, *10*, 558. [CrossRef]
17. Gaboriaud, R.J.; Veyssiere, P.; Rabier, J.; Böisson, M. Plasticity of monocrystalline yttrium oxide (Y_2O_3) at 0.45 T_m. *J. Mater. Sci.* **1978**, *13*, 907–990. [CrossRef]
18. Niu, D.; Ashcraft, R.W.; Chen, Z.; Stemmer, S.; Parsons, G.N. Chemical, physical, and electrical characterizations of oxygen plasma assisted chemical vapor deposited yttrium oxide on silicon. *J. Electrochem. Soc.* **2003**, *150*, F102–F109. [CrossRef]
19. Nieminen, M.; Sajavaara, T.; Rauhala, E.; Putkonen, M.; Niinistö, L. Surface-controlled growth of $LaAlO_3$ thin films by atomic layer epitaxy. *J. Mater. Chem.* **2001**, *11*, 2340–2345. [CrossRef]
20. Barve, S.; Deo, M.; Kar, R.; Sreenivasan, N.; Kishore, R.; Biswas, A.; Bhanage, B.; Rao, M.; Gantayet, L.M.; Patil, D. Microwave ECR Plasma Assisted MOCVD of Y_2O_3 Thin Films Using $Y(tod)_3$ Precursor and Their Characterization. *Plasma Process. Polym.* **2011**, *8*, 740–749. [CrossRef]
21. Kukli, K.; Ritala, M.; Pilvi, T.; Sajavaara, T.; Leskelä, M.; Jones, A.C.; Aspinall, H.C.; Gilmer, D.C.; Tobin, P.J. Evaluation of a praseodymium precursor for atomic layer deposition of oxide dielectric films. *Chem. Mater.* **2004**, *16*, 5162–5168. [CrossRef]
22. Triyoso, D.H.; Hedge, R.I.; Grant, J.M.; Schaeffer, J.K.; Roan, D.; White, B.E., Jr.; Tobin, P.J. Lanthanum aluminate by atomic layer deposition and molecular beam epitaxy. *J. Vac. Sci. Technol. B* **2005**, *23*, 288. [CrossRef]
23. Niinistö, J.; Putkonen, M.; Niinistö, L. Processing of Y_2O_3 Thin Films by Atomic Layer Deposition from Cyclopentadienyl-Type Compounds and Water as Precursors. *Chem. Mater.* **2004**, *16*, 2953–2958. [CrossRef]
24. Leskela, M.; Ritala, M. Magnesium aluminate thin films by atomic layer deposition from organometallic precursors and water. *J. Phys. IV* **1999**, *9*, Pr8–Pr837.

25. Seppälä, S.; Niinistö, J.; Blanquart, T.; Kaipio, M.; Mizohata, K.; Räisänen, J.; Lansalot-Matras, C.; Ritala, W.N.M.; Leskelä, M. Heteroleptic cyclopentadienyl-amidinate precursors for atomic layer deposition (ALD) of Y, Pr, Gd, and Dy oxide thin films. *Chem. Mater.* **2016**, *28*, 5440–5449. [CrossRef]

26. Majumder, P.; Jursich, G.; Kueltzo, A.; Takoudis, C. Atomic layer deposition of Y_2O_3 films on silicon using *tris* (ethylcyclopentadienyl) yttrium precursor and water vapor. *J. Electrochem. Soc.* **2008**, *155*, G152. [CrossRef]

27. de Rouffignac, P.; Yousef, A.; Kim, K.H.; Gordon, R. ALD of scandium oxide from scandium tris (N, N′-diisopropylacetamidinate) and water. *Electrochem. Solid State Lett.* **2006**, *9*, F45–F48. [CrossRef]

28. Karle, S.; Dan, V.S.; Prenzel, M.; Rogall, D.; Becker, H.-W.; Devi, A. Metal-organic CVD of Y_2O_3 Thin Films using Yttrium *tris*-amidinates. *Chem. Vap. Depos.* **2015**, *21*, 335–342. [CrossRef]

29. Milanov, A.P.; Xu, K.; Cwik, S.; Parala, H.; de los Arcos, T.; Becker, H.W.; Rogalla, D.; Cross, R.; Pauld, S.; Devi, A. Sc_2O_3, Er_2O_3, and Y_2O_3 thin films by MOCVD from volatile guanidinate class of rare-earth precursors. *Dalton Trans.* **2012**, *41*, 13936. [CrossRef]

30. Mai, L.; Boysen, N.; Subas, E.; de los Arcos, T.; Rogalla, D.; Grundmeier, G.; Bock, C.; Lu, H.L.; Devi, A. Water assisted atomic layer deposition of yttrium oxide using *tris*(N,N′-diisopropyl-2-dimethylamido-guanidinato) yttrium(III): Process development, film characterization and functional properties. *RSC Adv.* **2018**, *8*, 4987. [CrossRef]

31. Xu, K.; Ramjith, R.; Laha, A.; Parala, H.; Milanov, A.P.; Fisher, R.A.; Bugiel, E.; Feydt, J.; Irsen, S.; Toader, T.; et al. Atomic Layer Deposition of Gd2O3 and Dy2O3: A Study of the ALD Characteristics and Structural and Electrical Properties. *Chem. Mater.* **2012**, *24*, 651–658. [CrossRef]

32. Kaur, P.; Mai, L.; Muriqi, A.; Zanders, D.; Ghiyasi, R.; Safdar, M.; Boysen, N.; Winter, M.; Nolan, M.l.; Karppinen, M.; et al. Rational Development of Guanidinate and Amidinate Based Cerium and Ytterbium Complexes as Atomic Layer Deposition Precursors: Synthesis, Modeling, and Application. *Chem. Eur. J.* **2021**, *27*, 1–15.

33. Boysen, N.; Zanders, D.; Berning, T.; Beer, S.M.J.; Rogalla, D.; Bock, C.; Devi, A. Atomic layer deposition of dielectric Y_2O_3 thin films from a homoleptic yttrium formamidinate precursor and water. *RSC Adv.* **2021**, *11*, 2565–2574. [CrossRef]

34. Hitzbleck, J.; O'Brien, A.Y.; Deacon, G.B.; Ruhlandt-Senge, K. Role of donor and secondary interactions in the structures and thermal properties of alkaline-earth and rare-earth metal pyrazolates. *Inorg. Chem.* **2006**, *45*, 10329–10337. [CrossRef]

35. Myllimäki, P.; Nieminen, M.; Niinisto, J.; Putkonen, M.; Kukli, K.; Niinisto, L. High-permittivity $YScO_3$ thin films by atomic layer deposition using two precursor approaches. *J. Mater. Chem.* **2006**, *16*, 563–569. [CrossRef]

36. Cho, G.Y.; Noh, S.; Lee, Y.H.; Ji, S.; Cha, S.W. Study of Y_2O_3 thin film prepared by plasma enhanced atomic layer deposition. *ECS Trans.* **2014**, *64*, 15. [CrossRef]

37. Elder, J.P. Sublimation measurements of pharmaceutical compounds by isothermal thermogravivletry. *J. Therm. Anal.* **1997**, *49*, 897. [CrossRef]

38. Price, D.M. Vapor pressure determination by thermogravimetry. *Thermochim. Acta* **2001**, *367–368*, 253–262. [CrossRef]

39. Barry, S. Amidinates, guanidinates and iminopyrrolidinates: Understanding precursor thermolysis to design a better ligand. *Coord. Chem. Rev.* **2013**, *257*, 3192–3201. [CrossRef]

40. Riley, P.E.; Hanson, D.A. Comparison of etch rates of silicon nitride, silicon dioxide, and polycrystalline silicon upon O_2 dilution of CF_4 plasmas. *J. Vac. Sci. Technol.* **1989**, *B7*, 1352. [CrossRef]

41. Azimi, G.; Dhiman, R.; Kwon, H.M.; Paxson, A.T.; Varanasi, K.K. Hydrophobicity of rare-earth oxide ceramics. *Nat. Mat.* **2013**, *12*, 315–320. [CrossRef]

42. Caoa, Y.C.; Zhao, L.; Luo, J.; Wang, K.; Zhang, B.P.; Yokota, H.; Ito, Y.; Li, J.F. Plasma etching behavior of Y_2O_3 ceramics: Comparative study with Al_2O_3. *Appl. Surf. Sci.* **2016**, *366*, 304–309. [CrossRef]

43. Oh, I.K.; Kim, K.; Lee, Z.; Ko, K.Y.; Lee, C.W.; Lee, S.J.; Lansalot-Matras, J.M.M.C.; Noh, W.; Dussarrat, C.; Kim, H.; et al. Hydrophobicity of rare earth oxides grown by atomic layer deposition. *Chem. Mater.* **2015**, *27*, 148–156. [CrossRef]

44. Zhao, B.; Mattelaer, F.; Rampelberg, G.; Dendooven, J.; Detavernier, C. Thermal and plasma-enhanced atomic layer deposition of yttrium oxide films and the properties of water wettability. *ACS Appl. Mater. Interfaces* **2020**, *12*, 3179–3187. [CrossRef] [PubMed]

45. Külah, E.; Marot, L.; Steiner, R.; Romanyuk, A.; Jung, T.A.; Wäckerlin, A.; Meyer, E. Surface chemistry of rare-earth oxide surfaces at ambient conditions: Reactions with water and hydrocarbons. *Sci. Rep.* **2017**, *7*, 43369. [CrossRef]

46. Lundy, R.; Byrne, C.; Bogan, J.; Nolan, K.; Collins, M.N.; Dalton, E.; Enright, R. Exploring the role of adsorption and surface state on the hydrophobicity of rare earth oxides. *ACS Appl. Mater. Interfaces* **2017**, *9*, 13751–13760. [CrossRef]

47. Preston, D.J.; Miljkovic, N.; Sack, J.; Enright, R.; Queeney, J.; Wang, E.N. Effect of hydrocarbon adsorption on the wettability of rare earth oxide ceramics. *Appl. Phys. Lett.* **2014**, *105*, 011601. [CrossRef]